

Effective approach for area-based spaceborne SAR images registration using GLCM textural Features

Mohammad Amin Ghannadi^{1*}, Mohammad Saadatsresht², Saeedeh Alebooye², Moein Izadi³

¹ Department of Surveying Engineering, Arak University of Technology, Arak, Iran

² School of Surveying and Geospatial Engineering, College of Engineering, University of Tehran, Tehran, Iran

³ Department of Geological and Environmental Sciences, Western Michigan University Kalamazoo, MI, USA

Article history:

Received: 20 December 2019, Received in revised form: 4 April 2020, Accepted: 7 April 2020

ABSTRACT

Image registration is a very important step and an integral part of radargrammetry, interferometry, change detection, image fusion, etc. Because of noises and geometric challenges in synthetic aperture radar (SAR) images, the registration process is more complicated in these images in comparison to optical imagery. Moreover, one of the challenges in SAR image registration is to deal with weak textures. In this study, a multistep method was proposed for SAR image registration. In the proposed method, the use of grey level co-occurrence matrix (GLCM) textural features improved the output of regions with weak textures. The proposed method includes three main steps: first, as a pre-processing step, the speckle noise of SAR images was reduced through the refined Lee filter. Then, for each of the master and slave images, 10 GLCM textural features of original images were generated. Using each of the stereo textural feature images and Lucas-Kanade optical flow algorithms, one can determine the corresponding points. Finally, by considering some constraints, the coordinates of true matches were estimated. The precision of the proposed method was evaluated by the root mean square error (RMSE), Mean absolute error (MAE), and standard deviation (STD) criteria. Furthermore, the random sample consensus (RANSAC) -2D projective transformation method was used for accuracy evaluations. The results showed that the proposed method would generate more corresponding points compared to the two common registration methods, including template matching with normalized cross-correlation (NCC) and the traditional Lucas-Kanade optical flow. The proposed method improved the number of true matches up to 37% and 52% compared to the traditional LK and the template matching method, respectively.

KEYWORDS

Area-Based Registration
Space-Borne SAR Images
GLCM Textural Features
Lucas-Kanade Optical Flow

1. Introduction

SAR is a kind of microwave remote sensing imaging that operates under all weather conditions, during the day or at night. In recent years, SAR imaging has become one of the main detecting technologies that compensate for the defects of other kinds of imaging, such as infrared and optical imageries (Zhu et al., 2016). SAR imaging has numerous applications in radargrammetry (Capaldo et al., 2015), interferometry (Hu et al., 2008; Monserrat, Crosetto & Luzi 2014; González & Bräutigam, 2015; Samiei Esfahany &

Hanssen, 2018), classification, change detection (Hou et al., 2014), image fusion and image segmentation (Attarzadeh & Amini, 2019). SAR image registration, which is very challenging, is one of the main processing steps that is taken in all of the applications mentioned above. The challenge comes from the existence of speckle noise in SAR imagery and the availability of different configurations of these images (Wang et al., 2015). Image textures are classified into two different types: weak textures and strong textures (Haralick, 1979). A challenge in image registration is the

* Corresponding author

E-mail addresses: m.ghannadi@arakut.ac.ir (M.A. Ghannadi); msaadat@ut.ac.ir (M. Saadatsresht); s.alebooye@ut.ac.ir (S. Alebooye); moein.izadi@wmich.edu (M. izadi)

DOI: 10.22059/eoge.2020.295166.1070

existence of some poorly textured regions in images (Dellen & Wörgötter, 2009). In this study, a method for area-based SAR image registration is proposed, which is based on image texture analysis. In the proposed method, GLCM textural features are used for decreasing texture weakness in poorly textured regions. One of the challenges in the texture of SAR images is shadow. There is no information in shadow areas. The proposed method does not provide a solution to the shadow challenge in particular. It is, however, suitable for areas with image contents.

Matching approaches are classified into two main categories: area-based matching (ABM) and feature-based matching (FBM) methods (Wang et al., 2015). However, in some applications, hybrid methods are considered as well (Eftekhari et al., 2013). Owing to the use of image windows similarity in local ABM technique (Remondino et al., 2014), these methods are not usually suitable for images that contain periodic texture on some parts of them. In window-based methods, poorly textured areas result in mismatches (Hornberg, 2017). In FBM algorithms, since the interesting features such as points and lines have to be found in poorly textured areas, these methods will not operate properly. On the other hand, FBM methods are more suitable for sparse matching. These methods are practical in image processing and computer vision applications (Zhang & Lu, 2004; Cristinacce & Cootes, 2008). In order to improve the robustness and adaptability of SAR image registration, FBM methods are often used (Chen, Chen, & Su, 2014). In overlapping images, these methods are applied to finding an optimal spatial transformation to match the feature point coordinates, one after the other. Each of the matching methods has its application according to the type of the required outputs. For example, in producing digital elevation models (DEM) and generating dense point clouds, ABM methods are preferred. However, for image mosaicking and sparse point cloud generation, FBM methods are more likely to be used. The proposed method in this paper is suitable for both of the FBM and ABM methods.

Some previous research studies in SAR image registration have tried to introduce methods for improving radargrammetry processing. NCC is considered as one of the most popular criteria in ABM methods (Capaldo et al., 2015; Balz, Zhang, & Liao, 2013; Toutin et al., 2013; Wang, Yu, & Yu, 2012). NCC can be improved using a multi-size window, expanded window (Méric, Fayard, & Pottier, 2011), GLCM textural features (Yu et al. 2013), and Sum of Adaptive Normalized Cross-Correlation (SANCC) criteria (Ding et al., 2017). In addition to registration strategies that have been presented to improve the performance of radargrammetry, SAR image registration methods have been presented for improving interferometric processing (Hu et al., 2008; Natsuaki & Hirose, 2013). Beside ABM methods, which are usually applied for generating DEM or producing

land deformation measurements, FBM methods are commonly used and mostly applied in the registration process (Zhu et al., 2016; Fan et al., 2017; Chen, Chen, & Su, 2014; Wang et al., 2015). Among FBM algorithms, Scale-Invariant Feature Transform (SIFT), (Fan et al., 2015; Zhou et al., 2017; Wang et al., 2015; Gong et al., 2014; Liu et al., 2016; Dubois et al., 2017) and Speeded Up Robust Feature (SURF) (Suri et al., 2010) are the most common methods, whereas the methods that are based on local binary pattern descriptors (Ghannadi, 2013; Ghannadi & Saadatseresht, 2018) are also utilized for sparse matching. Some geometrical constraints, such as epipolar geometry, can be considered in improving the precision and efficiency of the process (Méric, Fayard, & Pottier, 2011; Gutjahr et al., 2014; Saadatseresht & Ghannadi, 2018). However, in several state-of-the-art methods, speckle noise was posed as a common challenge. Speckle noise can be reduced through a pre-processing step or within the registration process (Capaldo et al., 2015). A modified optical flow algorithm has been proposed for SAR image registration. By adapting the eFolki parameters, such as the size of the search window and the scale level for radar images, subject to speckle noise, the result is conclusive for co-registration of high-resolution urban SAR images (Lee et al., 1994). There is no specific solution that improves the weak texture of images in the research studies, as mentioned earlier, to make the registration process more efficient. In our proposed method, the use of GLCM textural features improves the regions that have weak textures. It is demonstrated that image registration results are improved. Lucas-Kanade optical flow (LK method) is used for the area-based image registration process (Lucas and Kanade) and the experiments are carried out on four space-borne stereo images including TerraSAR-X, Sentinel-1, Envisat, and Radarsat-2. Improving registration results using GLCM textural features is appropriate in many SAR image applications such as radargrammetry (with sparse matching).

The remainder of the paper is organized as follows: Section 2 gives a background of the refined Lee filter, GLCM, and the traditional LK method. Then, a multistep method for SAR image registration is proposed in Section 3. Afterward, data and experiments are presented in Section 4, and the results and discussion are described in Section 5. Finally, Section 6 concludes the paper.

2. Background

In this section, a brief background of algorithms that are used in the proposed method is given. First, the refined Lee filter, which is a despeckling filter, is described. Then, the mathematical basics under the generation of GLCM textural features are explained. Finally, the LK method is described as to how it is applied for area-based image registration.

2.1. Refined Lee filter

The speckle effect that appears in SAR images as granular noises complicates the image interpretation and decreases the efficiency of information extraction. The preservation of the mean value of a distributed target is an important aspect of speckle filtering. The mean filter, the Maximum A-Posteriori (MAP) filter, the Frost filter, and the refined Lee filter maintain the mean value, while many other filters, such as the filter using the logarithmic transformation and the median filter are inferior. The refined Lee filter – adopted and verified by Lee (Lee et al., 1994) – is based on the multiplicative speckle model and is developed to overcome challenges of the mean filter. If x , y , and n are the input signal, output signal, and noise, then they can be related as:

$$y(i, j) = x(i, j) * n(i, j), \quad (1)$$

The mean and variance of the noise-free original image x can be estimated from the local mean and variance of the observed image y . Thus

$$\bar{y}(i, j) = \bar{x}(i, j) * \bar{n}(i, j), \quad (2)$$

and

$$\text{var}_x(i, j) = \frac{\text{var}_y(i, j) + \bar{y}^2(i, j)}{\sigma_y^2 + \bar{n}^2(i, j)} \quad (3)$$

where \bar{y} and $\text{var}_y(i, j)$ are approximated by the sliding window, mean and variance, respectively with the assumption that $\bar{n} = 1$, $E\{(x - \bar{x})^2\}$ can be minimized to yield the estimated noise-free image \hat{x} , i.e.

$$x(i, j) - \bar{x}(i, j) | k(i, j) [y(i, j) - \bar{y}(i, j)], \quad (4)$$

where

$$k(i, j) = \frac{\text{var}_x(i, j)}{x(i, j)\sigma^2(y) + \text{var}_x(i, j)}$$

This indicates that in homogeneous regions, the local variance is close to zero. Thus, the filtered pixel is set to the average of pixels within the window. For high contrast areas or the edge regions, where the local variance seems to be usually larger, the pixel value is unchanged to maintain the feature. Although the assumption that $\bar{n}(i, j) = 1$ is made in this method, this limitation is not severe, since any other value of \bar{n} can be factored into the equation above. The value of σ_y , which is a measure of speckle strength, can be estimated by Equation (5).

$$\sigma_y = \frac{\sqrt{\text{var}_y}}{E[y]} \quad (5)$$

The refined Lee filter is the most famous despeckling filter. It will be used for the pre-processing of SAR images because

it reduces the speckle noise in the homogenous regions. The refined Lee filter is superior for visual interpretation because of its ability to maintain edges, linear features, point features, and texture information (Lee et al., 1994). In the next section, the theoretical concept of 10 GLCM textural features will be described.

2. GLCM

Considering the poor In statistical texture analysis, texture features are determined from the statistical distribution of observed combinations of intensities in a certain position relative to each other in the image. According to the number of pixels in each combination, statistics are classified into first-order, second-order, and higher-order statistics. GLCM is a procedure of extracting second-order statistical texture features. The approach has been used in several applications (Izadi, Mohammadzadeh, & Haghhighattalab, 2017). A GLCM is a matrix where the number of rows and columns is equal to the number of grey levels G in the image. The matrix element $P(i, j | \Delta x, \Delta y)$ is the relative frequency with which two pixels, separated by a pixel distance $(\Delta x, \Delta y)$, occur within a given neighborhood, one with intensity i and the other with intensity j . One may also state that the matrix element $P(i, j | d, \theta)$ contains the second-order statistical probability values for changes between grey levels i and j at a specific displacement. The parameters d and θ are distance and the specific angle, respectively. Given an $M \times N$ neighborhood of an input image containing G grey levels from 0 to $G - 1$, let $f(m, n)$ be the intensity at sample m , line n of the neighborhood. Then:

$$P(i, j | \Delta x, \Delta y) = WQ(i, j | \Delta x, \Delta y), \quad (6)$$

where

$$W = \frac{1}{(M - \Delta x)(N - \Delta y)}, \quad (7)$$

$$Q(i, j | \Delta x, \Delta y) = \sum_{n=1}^{N-\Delta x} \sum_{m=1}^{M-\Delta y} A, \quad (8)$$

and

$$A = \begin{cases} 1 & \text{if } f(m, n) = i \text{ \& } f(m + \Delta x, n + \Delta y) = j \\ 0 & \text{elsewhere} \end{cases} \quad (9)$$

Many texture features may be extracted from the GLCM (Haralick, 1979); the below notations are used here:

G is the number of grey levels used.

μ is the mean value of P .

μ_x, μ_y, σ_x and σ_y are the means and standard deviations of P_x and P_y . $P_x(i)$ is the i th entry in the marginal-probability matrix gained by summing the rows of $P(i, j)$:

$$P_x(i) = \sum_{j=0}^{G-1} P(i, j), \quad (10)$$

$$P_y(j) = \sum_{i=0}^{G-1} P(i, j), \quad (11)$$

$$\mu_x = \sum_{i=0}^{G-1} \sum_{j=0}^{G-1} iP(i, j) = \sum_{i=0}^{G-1} iP_x(i), \quad (12)$$

$$\mu_y = \sum_{i=0}^{G-1} \sum_{j=0}^{G-1} jP(i, j) = \sum_{j=0}^{G-1} jP_y(j), \quad (13)$$

$$\sigma_x^2 = \sum_{i=0}^{G-1} (i - \mu_x)^2 \sum_{j=0}^{G-1} P(i, j) = \quad (14)$$

$$\sum_{i=0}^{G-1} (P_x(i) - \mu_x(i))^2, \quad (15)$$

$$\sigma_x^2 = \sum_{i=0}^{G-1} (i - \mu_x)^2 \sum_{j=0}^{G-1} P(i, j) =$$

$$\sum_{i=0}^{G-1} (P_x(i) - \mu_x(i))^2,$$

and

$$P_{x+y}(k) = \sum_{i=0}^{G-1} \sum_{j=0}^{G-1} P(i, j) \quad i + j = k, \quad (16)$$

for $k = 0, 1, \dots, 2(G-1)$

$$P_{x-y}(k) = \sum_{i=0}^{G-1} \sum_{j=0}^{G-1} P(i, j) \quad |i - j| = k \quad (17)$$

A list of GLCM textural features used in this research is shown in Table 1.

In order to simplify the computation process, usually, the normalized values of the co-occurrence matrix are used. Some parameters represent certain features such as homogeneity, contrast, or regularized structures in the image. Although these features contain some information about texture, it is not easy to determine which characteristics of texture they are representing. Besides the primary image, the reason behind deploying these ten texture features is that these features cover an acceptable range of GLCM textural features characteristics. However, it is possible to include other features in the list to achieve better results. The next part explains the LK method, which is the image registration algorithm used in this paper.

2.2. Lucas-Kanade optical flow

In this section, the LK method is described. This approach was first outlined in 1981 for point tracking (Lucas & Kanade, 1981). In this study, it is applied for the image registration process.

Table 1. GLCM textural features used in this paper

ASM	$\sum_{i=0}^{G-1} \sum_{j=0}^{G-1} \{P(i, j)\}^2$
Contrast	$\sum_{n=0}^{G-1} n^2 \left\{ \sum_{i=1}^G \sum_{j=1}^G P(i, j) \right\}, n = i - j , i \neq j$
Entropy	$-\sum_{i=0}^{G-1} \sum_{j=0}^{G-1} P(i, j) \times \log(P(i, j))$
Homogeneity	$\sum_{i=0}^{G-1} \sum_{j=0}^{G-1} \frac{P(i, j)}{1 + (i, j)^2}$
Variance	$\sum_{i=0}^{G-1} \sum_{j=0}^{G-1} (i - \mu)^2 P(i, j)$
Dissimilarity	$\sum_{i=0}^{G-1} \sum_{j=0}^{G-1} i - j P(i, j)$
Mean	$\mu_x = \sum_{i=0}^{G-1} \sum_{j=0}^{G-1} iP(i, j), \mu_y = \sum_{i=0}^{G-1} \sum_{j=0}^{G-1} jP(i, j)$
Energy	$\left(\sum_{i=0}^{G-1} \sum_{j=0}^{G-1} P(i, j)^2 \right)^{\frac{1}{2}}$
Correlation	$\sum_{i=0}^{G-1} \sum_{j=0}^{G-1} \frac{(i - \mu_x)(j - \mu_y)}{\sigma_x \sigma_y} P(i, j)$
Max	the largest $P(i, j)$ value found within the window

Suppose that there are two images I_1 and I_2 of a dynamic scene that are separated in time and view by a short interval, implying that the object will not have changed extremely. If a pixel (x, y) in I_1 moves to $(x + u, y + v)$ in I_2 , it can be assumed that u and v are small; it can be also assumed that the pixel remains unaltered in appearance (intensity). Therefore:

$$I_2(x + u, y + v) - I_1(x, y) = 0 \quad (18)$$

Since the displacement is small, a linear approximation to $I_2(x + u, y + v)$ via a Taylor expansion can be made:

$$I_2(x+u, y+v) \approx I_2(x, y) + \frac{\partial I_2}{\partial x} u + \frac{\partial I_2}{\partial y} v, \quad (19)$$

combining Equation (18) and (19) gives:

$$I_2(x, y) - I_1(x, y) + \frac{\partial I_2}{\partial x} u + \frac{\partial I_2}{\partial y} v = 0, \quad (20)$$

an equation connecting the temporal and spatial differences around (x, y) , in which u and v are unknown. For the $n \times n$ window centred at (x, y) moves (u, v) between frames, and does not change in intensity, then Equation (20) provides n^2 linear equations for the two unknowns and the system is now overdetermined. It can be constructed an $n^2 \times 2$ matrix A , each row of that is an estimate of $\left(\frac{\partial I_2}{\partial x}, \frac{\partial I_2}{\partial y}\right)$ at respective pixels, and an $n^2 \times 1$ vector b , each component of that is the difference in intensities between I_1, I_2 at respective pixels:

$$A \begin{pmatrix} u \\ v \end{pmatrix} = b, \quad (21)$$

a least-squares best solution to this system is then available from:

$$A^T A \begin{pmatrix} u \\ v \end{pmatrix} = A^T b, \quad (22)$$

which is a 2×2 system, solvable if $A^T A$ is invertible.

Writing for brevity $I_x = \frac{\partial I_2}{\partial x}$ (and similar), it can be seen that:

$$A^T A = \begin{pmatrix} \sum I_{xx} & \sum I_{xy} \\ \sum I_{yx} & \sum I_{yy} \end{pmatrix} \quad (23)$$

Also, eigenvalues (λ_1, λ_2) of $A^T A$ should not be too small,

and it should be well-conditioned, meaning that $\frac{\lambda_1}{\lambda_2}$ should

not be too large ($\lambda_1 =$ larger eigenvalue) (Sonka, Hlavac, & Boyle, 2014). In the following section, a method for SAR image registration using the LK method and GLCM textural features is proposed.

3. Proposed method

Considering weakness and periodic texture in some regions of SAR intensity images, it is possible to use different textural features for image registration, each containing various characteristics that might be able to improve results. This is the core idea of our proposed method, and the steps are as follows: first, as a pre-processing step, the speckle

noise of SAR images is reduced through the refined Lee filter. Then, for each of the master and slave images, 10 GLCM textural features of original images are generated. Using each of the stereo feature images and the LK method, the corresponding points will be determined. Finally, considering some constraints, the coordinates of true matched points are estimated. Each of these steps is explained in details:

- 1) Reducing speckle noise using the refined Lee filter

First, using the refined Lee filter, the speckle noise of SAR images is reduced. One important aspect of this filter is preserving the mean value of a distributed target besides reducing speckle noise. The filter is applied to master and slave images, and then the despeckled images are used as inputs in step 2.

- 2) Generating GLCM textural features and finding corresponding points.

For each of the master and slave images, 10 textural features including ASM, contrast, entropy, homogeneity, variance, dissimilarity, mean, energy, correlation, and max images are generated. Then, the registration process is applied between each of the stereo images using the LK method. In other words, the registration process is applied 10 times for GLCM stereo images and once for the original stereo images. Thus, for each desired pixel (x_m, y_m) of the master image, 11 different corresponding coordinates $\{(x_1, y_1), (x_2, y_2), \dots, (x_{11}, y_{11})\}$ are found on slave images. In the next step, coordinates of the corresponding point (x_s, y_s) for point (x_m, y_m) and geometric and radiometric constraints are estimated using these 11 coordinates.

- 3) Estimating corresponding points.

In previous steps, 11 different coordinates were matched in slave images. However, they may have low accuracy and precision. In this step, using parallax, image content, and three sigma test (3σ) constraints, the points which are suitable for the final estimation of the corresponding point are determined. The aforementioned constraints will be explained in detail. The points which fulfill all of the above constraints will participate in the final estimation of the corresponding point.

- Parallax constraint: In some regions of SAR imagery, weak texture or periodic patterns are found. Although feature images can improve texture in some regions of the original images, all of the image regions may not improve necessarily. Therefore, the results of the registration process may not be correct. Using this constraint, blunders will be detected and removed from 11 generated coordinates.

Threshold values for x point parallax (p_x) and y point parallax (p_y) to estimate the accuracy of matched points are user-defined values.

For $i = 1, 2, \dots, 11$, point (x_{si}, y_{si}) is defined as blunder if:

$$x_{si} - x_m > p_{x_{operator}} \quad \text{or} \quad y_{si} - y_m > p_{y_{operator}} \quad (24)$$

- Image content constraint: After removing blunders using point parallax constraint, the coordinates that have appropriate local image content are utilized to estimate the corresponding point. Local image content in each region is determined using entropy. Assume that $w_{n \times n}$ is an image window with (x, y) as its central pixel. The image entropy E shows local image content:

$$E = \sum_{i=1}^{n^2} w_i \times \log\left(\frac{1}{w_i}\right), \quad (25)$$

Coordinates that have better image content in their local neighbors pass this step.

- Three sigma tests: The three sigma (standard deviation) test is applied to the rest of the coordinates in order to improve precision. This test is applied as the third constraint due to local displacements in coordinates in textural feature images.

σ is calculated from:

$$r_i = \sqrt{x_i^2 + y_i^2}, \quad (26)$$

$$V = \sqrt{\frac{\sum_{i=1}^m (r_i - \bar{r})^2}{m - 1}}, \quad (27)$$

$$\bar{r} = \frac{1}{m} \sum_{i=1}^m r_i, \quad (28)$$

m is the number of coordinates that have already passed the two previous constraints. So, if the condition in Equation (29) is true for (x_i, y_i) , it can be one of the final coordinates to estimate the corresponding point and otherwise, point (x_i, y_i) is a blunder and must be removed.

$$r_i - \bar{r} < 3\sigma \quad (29)$$

After finding the coordinates that satisfy all of the above constraints, their average value is used to estimate the final coordinates of the corresponding point. Assuming that l coordinates (x_i, y_i) from 11 initial coordinates have fulfilled the three constraints, the final coordinates of (x_s, y_s) from the slave image corresponding to (x_m, y_m) from the master image are estimated from:

$$x_s = \frac{\sum x_j}{l} \quad \& \quad y_s = \frac{\sum y_j}{l}, \quad (30)$$

Therefore, the process is carried out for all candidate points from the master image, and the corresponding points will be found in the slave image. The flowchart of the proposed method is shown in Figure 1.

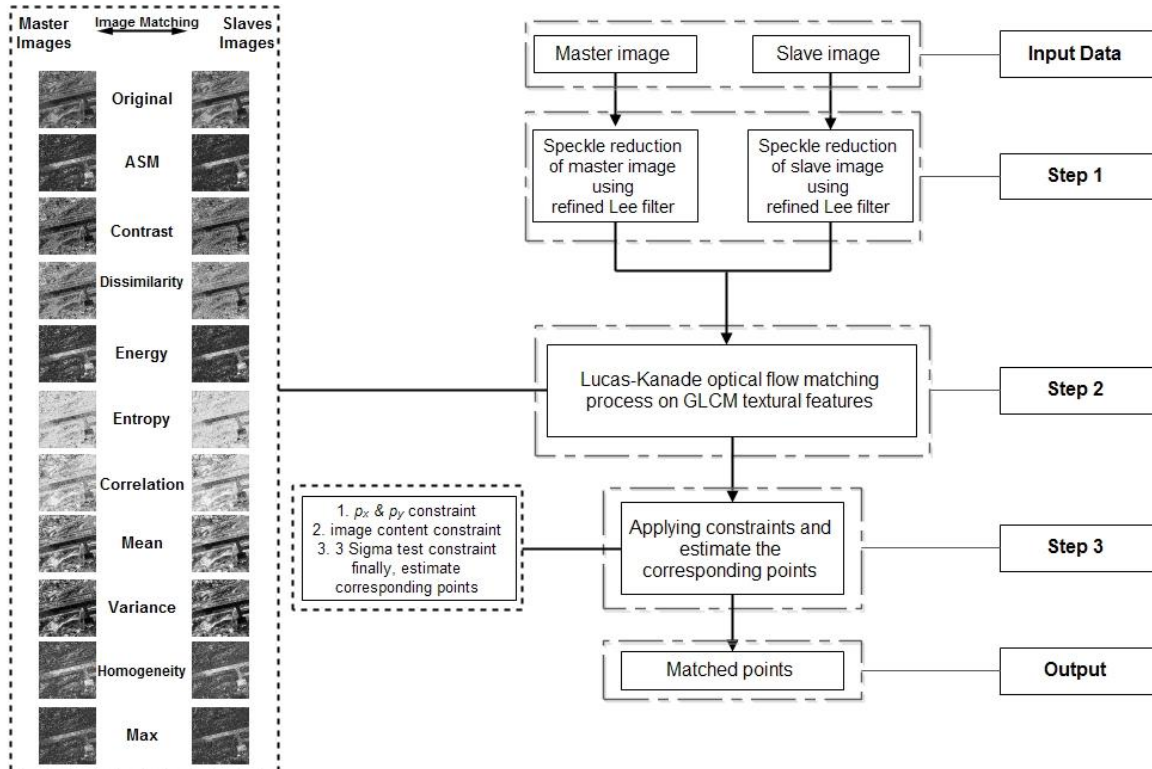


Figure 1. Flowchart of the proposed method.

Based on Figure (1), the steps of the proposed method are:

1. Despeckling of master and slave images using the Refined Lee filter.
2. Extracting GLCM textural images from each of the master and slave images, then matching each textural image pairs using the Lucas-Kanade method.
3. Applying the parallax, image content, and three sigma constraints on the results of the previous step and estimating the final matched points.

4. Data and experiment

Four spaceborne SAR datasets acquired from Envisat, Radarsat-2, TerraSAR-X, and Sentinel-1, are used in this experiment. These datasets are from Bam-Iran, Phoenix-United States, Jam-Iran, and Vancouver-Canada, respectively. Table 2. shows the specifications of the datasets. SAR images are in *.tiff format and Envisat, Radarsat-2, and TerraSAR-X images are in SLC level processing. Also, the GRDH format of Sentinel-1 images is used for the experiments. Since different regions in the datasets have various textures, the results of experiments in different regions should be considered. Therefore, each dataset experiment is conducted for three types of areas, including flat, mountainous, and urban areas. Figure 2 shows these areas in the master image. Each of the images includes 1000×1000 pixels. Table 2. shows that there is a variety of spatial resolution, imaging band, polarization, imaging mode, and time interval (from 11 to 71 days) in datasets. Different kinds of areas, including flat, mountainous, and urban areas, have been considered (Figure 2).

As mentioned earlier, the datasets include four SAR intensity image pairs obtained from TerraSAR-X, Radarsat-2, Sentinel-1, and Envisat. Experiments are conducted in different regions of these images, including flat, mountainous, and urban areas. Therefore, experiments are conducted on actually 12 image pairs with 1000×1000 pixels dimensions. An 80×80 grid of points (including 6400 points) on the master image is considered for the experiments. The

goal is to find the corresponding points on the slave image. After reducing speckle noise from the original image pairs, the traditional LK registration method and template matching are applied as the competing algorithms. This experiment is again conducted according to the proposed method (Figure 1), which means after reducing speckle noise and performing the LK method on 11 image pairs, the constraints described in Section 3 are applied. Image coordinates for the points within this grid are similar in all the master images, but their matched points are different on the slave images.

In the following, the tuning parameters of the proposed method are introduced. The window size for generating the GLCM textural features is determined as 11×11 pixels. As mentioned in Section 3, the first constraint in the proposed method is point parallax constraint. The threshold values for ρ_x and ρ_y are predetermined as 10 pixels. In other words, the corresponding points with ρ_x and ρ_y values larger than 10 pixels are considered as blunders. Furthermore, image content is the other constraint in the proposed method. In this study, 60% of the coordinates in which their neighbor window has better image content will be chosen.

In order to evaluate the results, two criteria have been considered for the proposed method: registration accuracy and precision. The RANSAC and 2D projective transformation method (Yang, Yu, & Zhang, 2014) was adopted for the accuracy assessment of the proposed method. For 6400 points from the master image, there are 6400 corresponding points in the slave image, some of which are false matches. RANSAC-2D projective transformation specifies blunders, so the percentage of success in determining corresponding points will be obtained. In order to determine the precision of assessment, root mean square error (RMSE), mean absolute error (MAE), and standard deviation (STD) criterion are utilized. In the next section, the results of the experiments are demonstrated and discussed.

Table 2. Specification of SAR datasets.

Images data	Location	Resolution	Band	Polarization	Acquisition mode	Orbit Direction	Acquisition Date
Envisat	Iran-Bam	30m	C	VV	Stripmap	Descending	2003/06/01-2003/08/04
Radarsat-2	US-Phoenix	2m	C	HH	Ultra-fine	Ascending	2008/05/04-2008/05/28
TerraSAR-X	Iran-Jam	1m	X	VV	Spotlight	Descending	2011/04/17-2011/04/28
Sentinel-1	Canada-Vancouver	20m	C	VV	Interferometric Wide	Descending	2018/01/05-2018/01/29

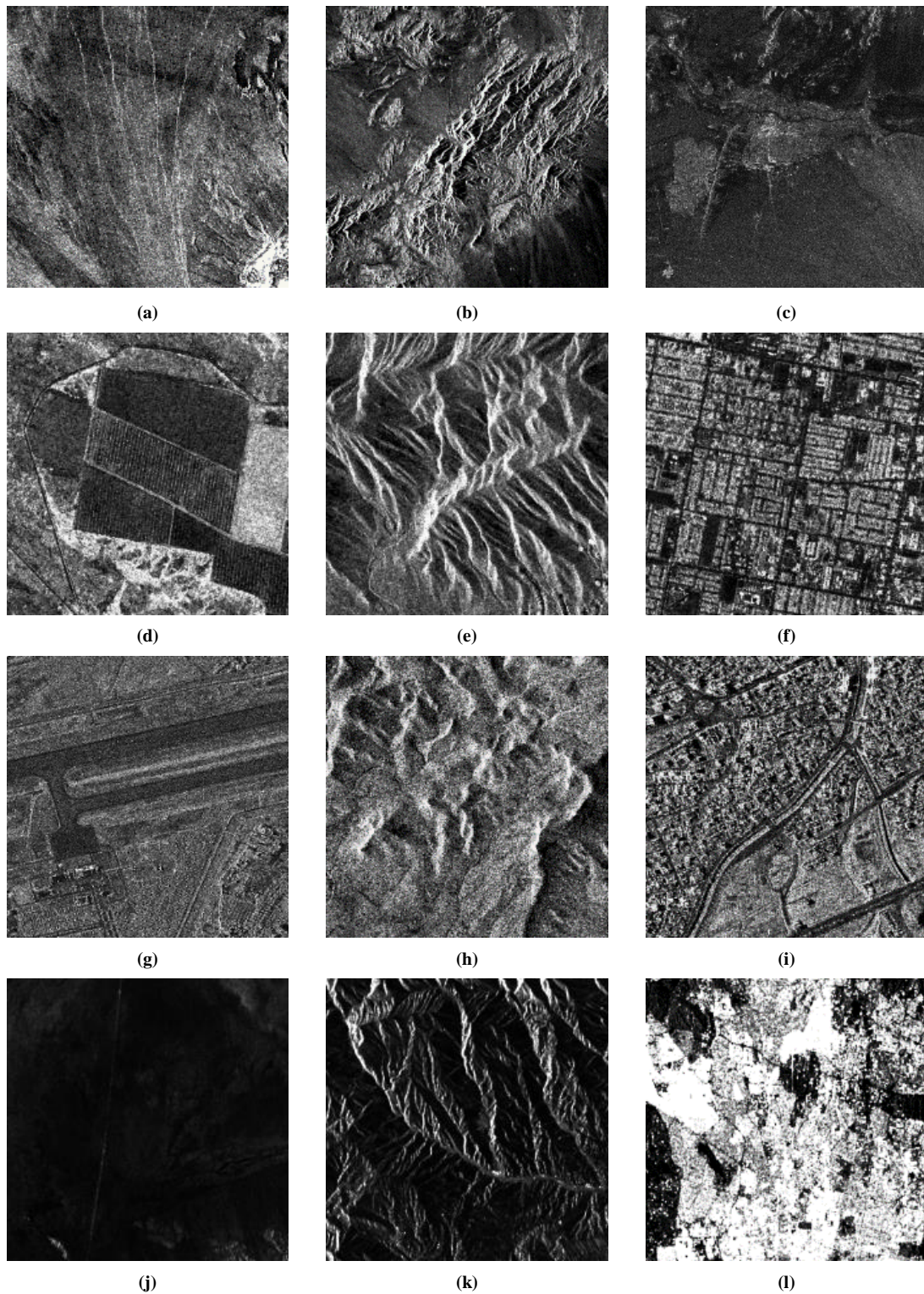


Figure 2. Different types of areas from Envisat (a, b, c), Radarsat-2 (d, e, f), TerraSAR-X (g, h, i) and Sentinel-1 (j, k, l).

5. Results and discussion

In this section, the results are shown and discussed. As described in Section 4, the experiments are conducted on 12 images with 1000×1000 pixels, including mountainous, urban, and flat areas. The experimental results based on

template matching and traditional LK are demonstrated in Table 3 and Table 4, respectively. Also, Table 5 shows the experimental results based on the proposed method implementation. The images are matched in image coordinates and are evaluated in the image space.

Table 3. Experimental results on original images using template matching+NCC.

Image Data	Region Type	Matched points number	Accuracy (%)	RMSE (pixel)	MAE (pixel)	STD (pixel)
Envisat	Flat	2113	33.02	1.06	0.97	0.30
	Mountain	5127	80.11	0.19	0.15	0.08
	Urban	4415	70	1.04	0.85	0.52
Sentinel-1	Flat	2799	43.73	1.29	1.21	0.79
	Mountain	4187	65.42	1.27	1.12	0.60
	Urban	5451	85.17	0.97	0.89	0.55
RadarSAT-2	Flat	3153	49.27	0.84	0.75	0.48
	Mountain	5988	93.56	0.96	0.84	0.59
	Urban	5748	89.81	0.59	0.48	0.26
TerraSAR-X	Flat	1911	29.86	0.99	0.87	0.50
	Mountain	4370	68.28	1.12	0.99	0.48
	Urban	6012	93.94	0.88	0.78	0.56

Table 4. Experimental results on original images using the traditional LK method.

Image Data	Region Type	Matched points number	Accuracy (%)	RMSE (pixel)	MAE (pixel)	STD (pixel)
Envisat	Flat	2890	45.15	1.22	1.11	0.49
	Mountain	6400	100	0.02	0.02	0.01
	Urban	4306	67.28	0.85	0.72	0.45
Sentinel-1	Flat	2924	45.69	1.2	1.09	0.48
	Mountain	4078	63.72	1.13	1.01	0.50
	Urban	5514	86.16	0.86	0.72	0.46
RadarSAT-2	Flat	3849	60.14	1.03	0.92	0.47
	Mountain	6326	98.84	0.81	0.69	0.42
	Urban	6349	99.20	0.65	0.55	0.34
TerraSAR-X	Flat	2850	44.50	1.01	0.89	0.48
	Mountain	4506	70.41	1.11	1	0.48
	Urban	5885	91.95	0.73	0.61	0.40

Table 5. Experimental results on images using the proposed method.

Image Data	Region Type	Matched points number	Accuracy (%)	RMSE (pixel)	MAE (pixel)	STD (pixel)
Envisat	Flat	5300	82.81	1.16	1.06	0.48
	Mountain	6400	100	0.03	0.03	0.02
	Urban	5525	86.33	1.22	1.12	0.49
Sentinel-1	Flat	2972	46.44	1.31	1.22	0.48
	Mountain	5838	91.22	1.18	1.07	0.50
	Urban	6086	95.09	1.03	0.91	0.48
RadarSAT-2	Flat	4556	71.19	1.21	1.11	0.48
	Mountain	6174	96.47	1.14	1.02	0.49
	Urban	6298	98.41	0.97	0.86	0.45
TerraSAR-X	Flat	5268	82.31	1.22	1.12	0.49
	Mountain	5197	81.20	1.20	1.10	0.48
	Urban	6319	98.73	0.86	0.74	0.43

Table 5 reveals that the use of textural feature images, as well as original images, has improved the accuracy of corresponding points. On the other hand, the GLCM textural feature images have improved the number of correct matches. Although it seems that the proposed method has slightly decreased the precision, comparing Table 5 with Table 3 and Table 4 shows that there is no significant difference in the precision criterion of the two experimental results. As it is shown, the use of original images from the mountainous areas of Envisat images leads to matching all 6400 points by the traditional LK method. It confirms that these images contain desirable textures. However, when using original image pairs from flat areas of Envisat, only 45% of the points from the master image have corresponded

in the slave image using traditional LK. As for template matching, however, this percentage goes down to 33%, which shows that traditional LK and template matching methods have not operated well due to the weak texture of original images. The percentage of success in the registration process improves to 83% when feature images are used in estimating correspondences of the flat area of Envisat. Figure 3 demonstrates the role of each textural feature in the improvement of TerraSAR X image registration in the flat area.

In Figure 3, these points have satisfied the constraints of the proposed method and are used in Equation (30). Figure 4 demonstrates true matched points using traditional LK, and true matched points using the proposed method.

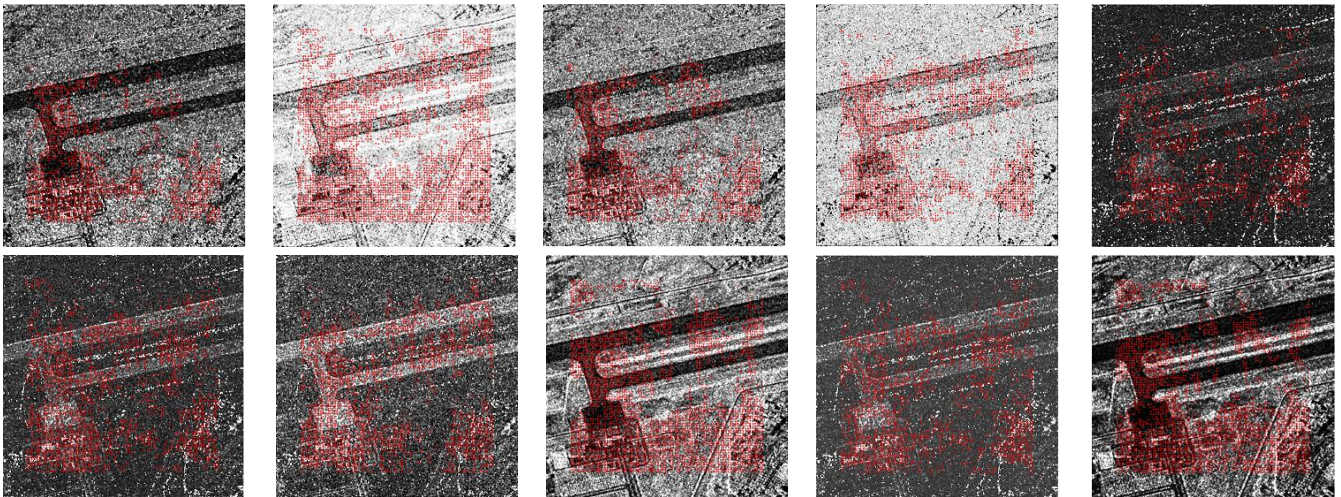


Figure 3. Role of textural features in improving TerraSAR-X image registration in the flat area.

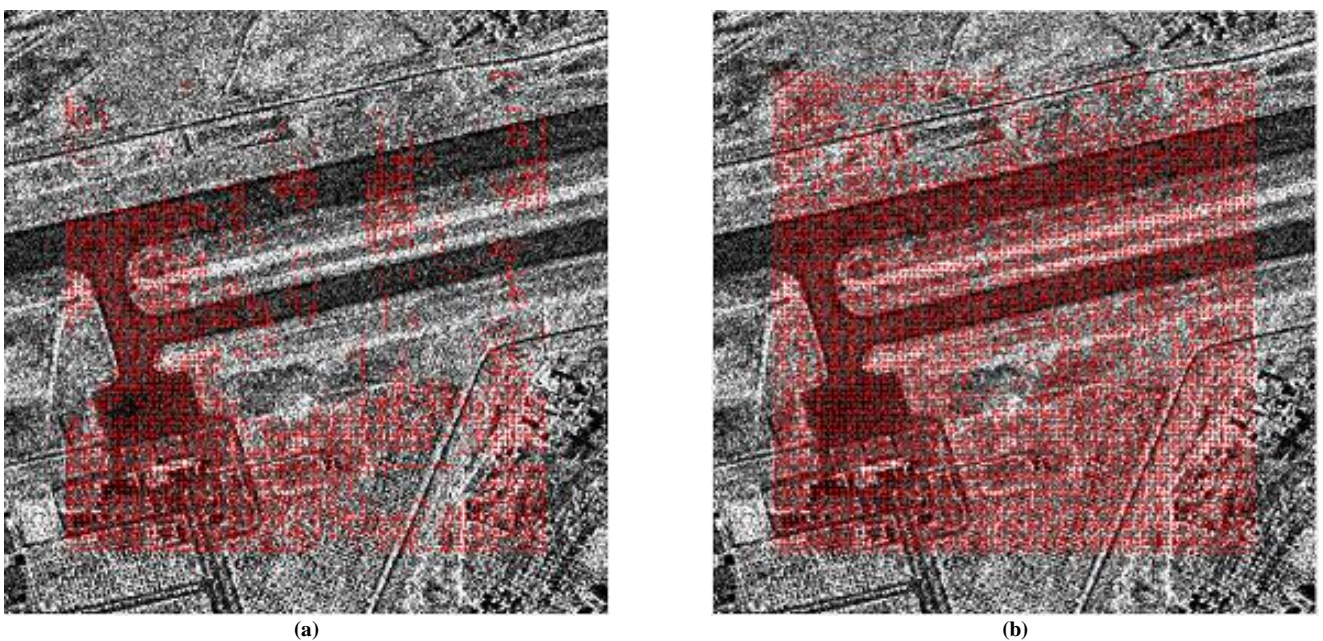


Figure 4. True matched points on original image using (a) traditional LK method and (b) the proposed method.

Also, Figure 5 highlights some points that could not be matched using the original image and its corresponding matched points in some textural feature images.

Figure 6 shows the numerical result in Table 3 to 5. The results confirm that the weakest textures belong to the flat areas. Furthermore, image texture in high-resolution images is better compared to low-resolution images. The proposed method has the highest precision in urban areas and the lowest precision in flat areas. As shown in Table 5, the main advantage of this method is increasing the number of true matches. It has mostly improved the results of registration, but in some cases, no significant improvements have been obtained. For example, in images from the flat areas of Sentinel-1, the proposed method has improved the

number of correct matches only 2%, compared to the traditional LK method. Other registration algorithms can replace the LK method.

However, this method is time consuming compared to traditional LK and original images. The process takes about 3 seconds with one image pair, while the proposed method takes about 35 seconds with the same hardware configuration. It can be concluded that when the number of true matches is more important than the processing time, the proposed method is preferred. The novelty of this study is the fusion of the results of feature image matching to improve the registration process.

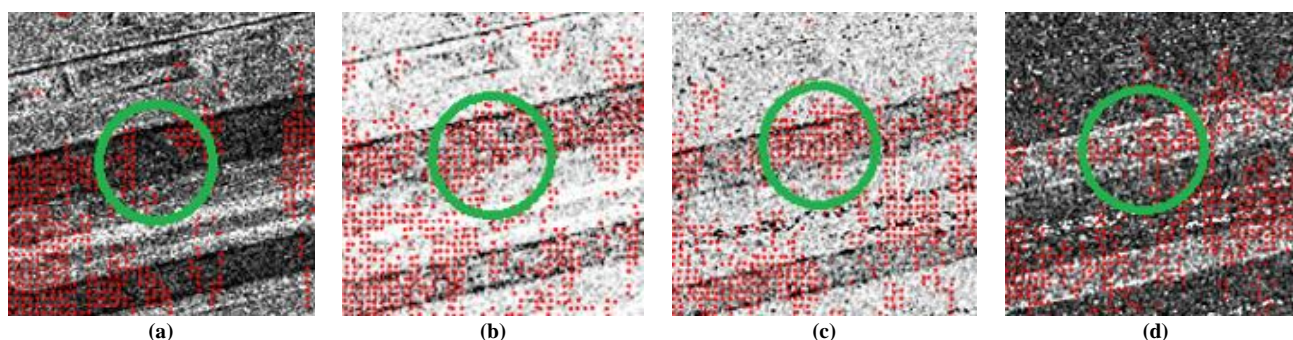


Figure 5. (a) Original image, (b) correlation image, (c) entropy image and (d) homogeneity image. Matching process failed using original images (a) information in the marked regions and some points are matched in same areas using textural features (b, c and d).

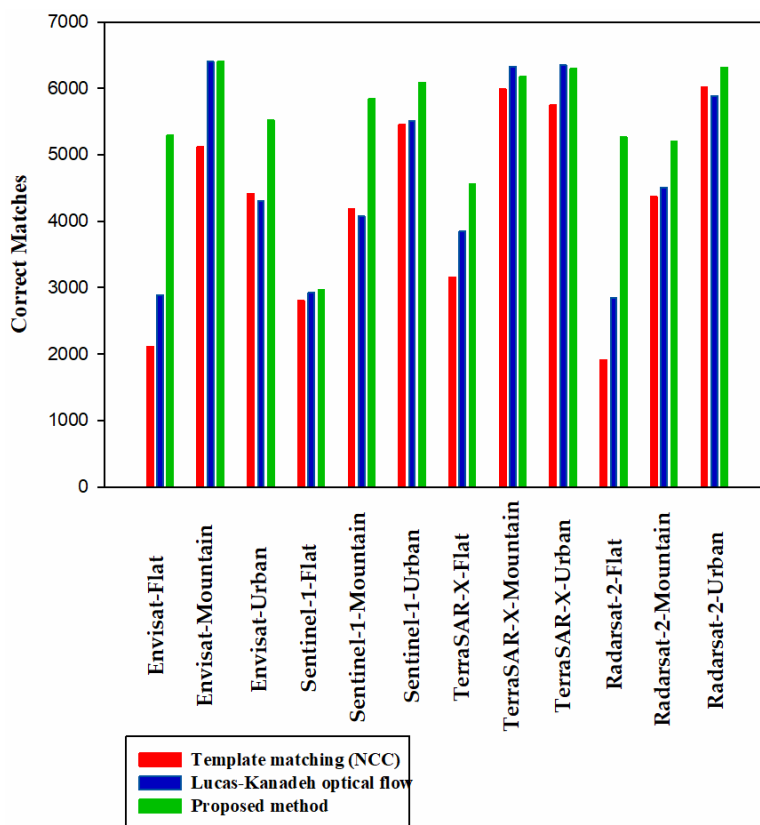


Figure 6. A graph bar of the experimental results.

6. Conclusion

Image registration is one of the most important processing steps that is taken in SAR images applications such as radargrammetry, interferometry, classification, image fusion, and change detection. The existence of weak textures in some regions of SAR imagery causes challenges in the image registration process. This study presented a method based on image texture analysis for area-based SAR images registration that uses GLCM textural features to improve weak texture in some regions of images. While in state-of-the-art research studies there is no solution to improve the weak texture of images in the matching process, the novelty of the presented method is decreasing the weak texture to improve SAR image registration.

The proposed method includes three major steps. First, speckle noise was reduced using the refined Lee filter. Afterward, for each master and slave images, 10 GLCM images were generated. Using these images, the LK method, and by applying three predetermined constraints, the corresponding points were established. The experiments were carried out on four satellite radar image pairs from TerraSAR-X, Sentinel-1, Envisat, and Radarsat-2, considering different regions of the images such as flat, mountainous, and urban areas. Then, the RANSAC-2D projective transformation method evaluated the accuracy of the method. Furthermore, the standard deviation determined the precision of the proposed method. The results demonstrated that the use of textural features, as well as original images, improves the registration process by up to 37%, compared to the traditional LK. This improvement is 52% higher than that of the template matching method. The advantage of the proposed method is increasing the correspondences in regions with weak texture. However, the processing time increases because of repeating the registration process between feature image pairs.

The proposed method is suitable for image registration in areas with image content. While there is not enough image information in the shadow areas, this study will be continued in the future to come up with a registration method to have a better performance in shadow areas.

References

- Attarzadeh, R., & Amini, J. (2019). "Towards an object-based multi-scale soil moisture product using coupled Sentinel-1 and Sentinel-2 data." *Remote Sensing Letters*, 10 (7), 619-28.
- Balz, T., Zhang, L., & Liao, M. (2013). "Direct stereo radargrammetric processing using massively parallel processing." *ISPRS Journal of Photogrammetry and Remote Sensing*, 79, 137-46.
- Capaldo, P., Nascetti, A., Porfiri, M., Pieralice, F., Fratarcangeli, F., Crespi, M., & Toutin, T. (2015). "Evaluation and comparison of different radargrammetric approaches for Digital Surface Models generation from COSMO-SkyMed, TerraSAR-X, RADARSAT-2 imagery: Analysis of Beauport (Canada) test site." *ISPRS Journal of Photogrammetry and Remote Sensing*, 100, 60-70.
- Chen, T., Chen, L., & Su, Y. (2014). "A SAR image registration method based on pixel migration of edge-point feature." *IEEE Geoscience and Remote Sensing Letters*, 11 (5), 906-10.
- Cristinacce, D., & Cootes, T. (2008). "Automatic feature localisation with constrained local models." *Pattern Recognition* 41(10), 3054-67.
- Dellen, B., & Wörgötter, F. (2009). "Disparity from stereo-segment silhouettes of weakly-textured images." *Paper presented at the 20'th British Machine Vision Conference*.
- Ding, H., Zhang, J., Huang, G., & Zhu, J. (2017). "An Improved Multi-Image Matching Method in Stereo-Radargrammetry." *IEEE Geoscience and Remote Sensing Letters*, 14(6), 806-10.
- Dubois, C., Nascetti, A., Thiele, A., Crespi, M., & Hinz, S. (2017). "SAR-SIFT for Matching Multiple SAR Images and Radargrammetry." *PFG – Journal of Photogrammetry, Remote Sensing and Geoinformation Science*, 85(3), 149-58.
- Eftekhari, A., Ghannadi M, A., Motagh, M., & Saadat Seresht, M. (2013). "3D object coordinates extraction by radargrammetry and multi step image matching." *International Archives of the Photogrammetry, Remote Sensing and Spatial Information Sciences*, 1:W3.
- Fan, J., Wu, Y., Li, M., Liang, W., & Zhang, Q. (2017). "SAR Image Registration Using Multiscale Image Patch Features With Sparse Representation." *IEEE Journal of Selected Topics in Applied Earth Observations and Remote Sensing*, 10(4), 1483-93.
- Fan, J., Wu, Y., Wang, F., Zhang, Q., Liao, G., & Li, M. (2015). "SAR image registration using phase congruency and nonlinear diffusion-based SIFT." *IEEE Geoscience and Remote Sensing Letters*, 12(3), 562-6.
- Ghannadi, M. A. Saadateseresh, M., & Motagh, M. (2013). "Using Multi Resolution Census and Ranklet Transformation in Long Base Line SAR Image Matching." *Isprs - International Archives of the Photogrammetry*, XL-1/W3, 181-4.
- Ghannadi, M., A., & Saadateseresh, M. (2018). "A Modified Local Binary Pattern Descriptor for SAR Image Matching." *IEEE Geoscience and Remote Sensing Letters*, 16(4), 568-572.
- Gong, M., Zhao, S., Jiao, L., Tian, D., & Wang, S. (2014). "A novel coarse-to-fine scheme for automatic image registration based on SIFT and mutual information." *IEEE Transactions on Geoscience and Remote Sensing*, 52 (7), 4328-38.
- González, C., & Bräutigam, B. (2015). "Relative Height Accuracy Estimation Method for InSAR-Based DEMs." *IEEE Journal of Selected Topics in Applied Earth Observations and Remote Sensing*, 8(11), 5352-60.
- Gutjahr, K., Perko, R., Raggam, H., & Schardt, M. (2014). "The epipolarity constraint in stereo-radargrammetric dem generation." *IEEE Transactions on Geoscience and Remote Sensing*, 52(8), 5014-22.

- Haralick, R., M. (1979). "Statistical and structural approaches to texture." *Proceedings of the IEEE*, 67(5), 786-804.
- Hornberg, A. (2017). *Handbook of Machine and Computer Vision: The Guide for Developers and Users*: John Wiley & Sons".
- Hou, B., Wei, Q., Zheng, Y., & Wang, S. (2014). "Unsupervised change detection in SAR image based on Gauss-log ratio image fusion and compressed projection." *IEEE Journal of Selected Topics in Applied Earth Observations and Remote Sensing*, 7(8), 3297-317.
- Hu, J., Li, Z., Ding, X., & Zhu, J. (2008). "Two-dimensional co-seismic surface displacements field of the Chi-Chi earthquake inferred from SAR image matching." *Sensors*, 8(10), 6484-95.
- Izadi, M., Mohammadzadeh, A., & Haghigattalab, A. (2017). "A new neuro-fuzzy approach for post-earthquake road damage assessment using GA and SVM classification from QuickBird satellite images." *Journal of the Indian Society of Remote Sensing*, 45(6), 965-77.
- Lee, J., Jurkevich, L., Dewaele, P., Wambacq, P., & Oosterlinck, A. (1994). "Speckle filtering of synthetic aperture radar images: A review." *Remote Sensing Reviews*, 8(4), 313-40.
- Liu, F., Bi, B., Chen, L., Shi, H., & Liu, W. (2016). "Feature-Area Optimization: A Novel SAR Image Registration Method." *IEEE Geoscience and Remote Sensing Letters*, 13(2), 242-6.
- Lucas, B., & Kanade, T. (1981). "An iterative image registration technique with an application to stereo vision.", 674.
- Méric, S., Fayard, F., & Pottier, E. (2011). "A multiwindow approach for radargrammetric improvements." *IEEE Transactions on Geoscience and Remote Sensing*, 49(10), 3803-10.
- Montserrat, O., Crosetto, M., & Luzi, G. (2014). "A review of ground-based SAR interferometry for deformation measurement." *ISPRS Journal of Photogrammetry and Remote Sensing*, 93, 40-8.
- Natsuaki, R., & Hirose, A. (2013). "InSAR local co-registration method assisted by shape-from-shading." *IEEE Journal of Selected Topics in Applied Earth Observations and Remote Sensing*, 6(2), 953-9.
- Remondino, F., Spera, M., G., Nocerino, E., Menna, F., & Nex, F. (2014). "State of the art in high density image matching." *The Photogrammetric Record* 29(146), 144-66.
- Saadatseresht, M., & Ghannadi, M., A. (2018). "Efficient Method for Outlier Removal in SAR Image Matching Based on Epipolar Geometry." *IET Radar, Sonar & Navigation*, 12(11), 1307-1312.
- Samiei Esfahany, S., & Hanssen, R. (2018). "Feasibility assessment of exploitation of distributed scatterers in InSAR stacks over pasture areas for different SAR satellite missions." *Earth Observation and Geomatics Engineering*, 2(2), 64-73.
- Sonka, M., Hlavac, V., & Boyle, R. (2014). *Image processing, analysis, and machine vision*: Cengage Learning".
- Suri, S., Schwind, P., Uhl, J., & Reinartz, P. (2010). "Modifications in the SIFT operator for effective SAR image matching." *International Journal of Image and Data Fusion*, 1(3), 243-56.
- Toutin, T., Blondel, E., Clavet, D., & Schmitt, C. (2013). "Stereo radargrammetry with Radarsat-2 in the Canadian Arctic." *IEEE Transactions on Geoscience and Remote Sensing*, 51(5), 2601-9.
- Wang, B., Zhang, J., Lu, L., Huang, G., & Zhao, Z. (2015). "A Uniform SIFT-Like Algorithm for SAR Image Registration." *IEEE Geoscience and Remote Sensing Letters*, 12(7), 1426-30.
- Wang, Y., Yu, Q., & Yu, W. (2012). "An improved Normalized Cross Correlation algorithm for SAR image registration." *IEEE International Geoscience and Remote Sensing Symposium (IGARSS)*, 2086-2089.
- Yang, H., Yu, M., & Zhang, S. (2014). "Wide baseline stereo matching based on scale invariant feature transformation with hybrid geometric constraints." *IET Computer Vision*, 8(6), 611-9.
- Yu, Q., Wang, Y., Zhang, Y., & Qu, G. (2013). "High performance local-texture-information weighted SAR template image matching." *IET International Radar Conferenc*, 0156-0156.
- Zhang, D., & Lu, G. (2004). "Review of shape representation and description techniques." *Pattern recognition*, 37(1), 1-19.
- Zhou, D., Zeng, L., Liang, J., & Zhang, K. (2017). "Improved method for SAR image registration based on scale invariant feature transform." *IET Radar, Sonar & Navigation*, 11(4), 579-85.
- Zhu, H., Ma, W., Hou, B., & Jiao, L. (2016). "SAR image registration based on multifeature detection and arborescence network matching." *IEEE Geoscience and Remote Sensing Letters*, 13(5), 706-10.